Exploiting Earth Observation data products for mapping Local Climate Zones

Zina Mitraka[1,3], Nektarios Chrysoulakis[1], Jean Philippe Gastellu-Etchegorry[2], Fabio Del Frate[3,4]
[1] *Foundation for Research and Technology Hellas, Greece, mitraka@iacm.forth.gr*
[2] Centre d'Etude Spatiale de la Biosphère, France, jean-philippe.gastellu-etchegorry@cesbio.cnes.fr
[3] Tor Vergata University of Rome, Italy
[4] Geo-K s.r.l., Italy, delfrate@disp.uniroma2.it

1. Introduction

The increasing availability of EO systems and the advances in remote sensing techniques have increased the opportunities for monitoring the urban environment and its thermal behaviour. Several parameters related to the urban climate can be derived from EO data, providing valuable support for advanced urban studies (Chrysoulakis, 2013; Xu et al., 2008). Voogt and Oke (2003), on a review on application of thermal remote sensing in the urban areas, highlighted the need to advance research beyond qualitative description of thermal patterns and simple correlations and suggested to avoid land use data to describe the urban surface and focus on more fundamental surface descriptors. Luyssaert et al. (2014) recently presented an example of Land Surface Temperature (LST) trend increase due to modification of the anthropogenic activities without changes in land-cover. Among others, Grimmond et al. (2010) highlight the need to explore the use of new measurement techniques including satellite systems. Moreover, coupling of different data sources, like EO and in-situ measurements and the development of synergistic methods are necessary to overcome individual weaknesses and benefit from their diversity (Chrysoulakis et al., 2013).

Recently, Stewart and Oke (2012) introduced a detailed classification scheme of Local Climate Zones (LCZ) based on various urban typologies, which explicitly defines urban landscapes according to their thermal properties. The scheme aims to be objective (incorporating measurable and testable features relevant to surface thermal climate), inclusive (sufficiently generic in its representation of local landscapes to not inherit regional or cultural biases) and standardized. The individual classes aim to have relatively homogenous air temperature within the canopy layer and they are defined by fact sheets with both qualitative and quantitative properties, including several features that can be derived from EO data.

A first attempt to capture LCZ from multiple EO data is presented by Bechtel and Danake (2012), while Bechtel et al. (2015) present the conceptual considerations regarding a protocol for standardizing LCZ derivation from multi-temporal Landsat imagery. Multiple EO data were used by Mitraka et al. (2015) to build a methodology to for LCZ mapping. See et al. (2015) present an example of the application of such a method for Dublin and explain the advances of exploiting crowdsourcing methods to apply the method globally. Lelovics et al. (2014) developed a semi-empirical GIS-based method for delineating the LCS in Szeged, Hungary. Gamba et al. (2012) on the other hand, developed a LCZ classification scheme based on very high resolution data satellite data. In this study, remote sensing techniques are applied to derive quantitative information, suitable for identifying LCZ. Parameters like the sky-view factor, the building density, the impervious and pervious surface fraction, the mean building/ tree height and the surface albedo are estimated for the city of Heraklion, Greece and a methodology was developed to combines them for LCZ identification, according to Stewart and Oke (2012).

2. Study areas and data

The study area is the city of Heraklion, Greece. It is a typical Mediterranean city, characterized by mixed land-use patterns that include residential, commercial and industrial areas, transportation networks and rural areas. Fig. 1 shows the Urban Atlas (Meirich, 2008) land use map of Heraklion, overlaid to Google Earth. Apart from the Heraklion city core, the rest of the study area is featuring mixed urban and agricultural land cover pattern, mainly olive trees and vineyards. The study area (around 50 km^2) is outlined by a dashed polygon in Fig. 1.

A Landsat-8 Level 1B image acquired over the study area on 19 June 2013 (08:55 UTC) was used. A Digital Surface Model (DSM) of 0.8 m and a Digital Terrain Model (DTM) of 5 m spatial resolution were available from the National Cadastre of Greece. Both DSM and DTM were produced using stereoscopic imagery from an airborne campaign. Information on the buildings footprint was also available from the National Statistical Service of Greece.

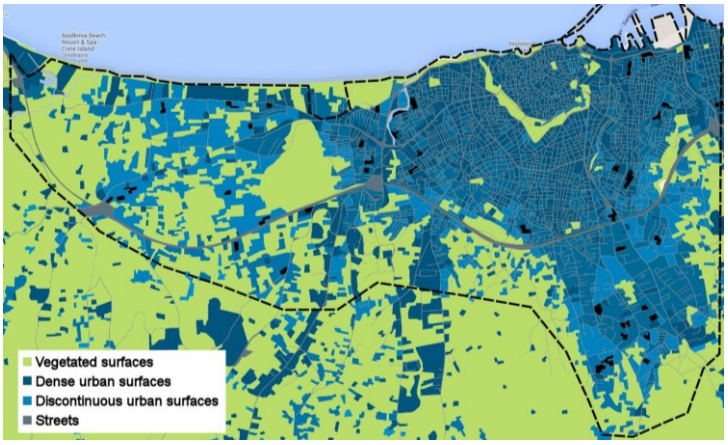

Fig. 1. Urban Atlas land use polygons overlaid to Google Maps of the study area (dashed line) in the city of Heraklion, Greece.

3. Methodology

The remote sensing methods used to derive the different parameters used for identifying the LCZ are briefly explained in this section, followed by the methodology developed to map the LCZ for the study area.

3.1 Sky-view factor

The sky-view factor represents the fraction of sky hemisphere visible from ground level. It varies with height and spacing of buildings and trees and it affects the radiational heating/cooling. The sky-view factor describes the ratio between the potential visible sky and the actual visible sky from a certain location, it depends on the height to width ratio of the street canyon and its values range between 0–1. There are some recent studies published that use EO data to estimate the sky-view factor (Lindberg and Grimmond, 2010; Rigo and Parlow, 2007). In this study, the sky-view factor was estimated in 0.8 m spatial resolution using the available DSM using the approach suggested by Lindberg and Grimmond (2010).

3.2 Building Density

Building density represents the proportion of ground surface with building cover. It affects the surface reflectivity, flow regimes and heat dispersion above ground. Various remote sensing methods exist that identify the buildings footprint from high resolution optical EO data or LiDAR data (Priestnall et al., 2000), from which building density can then be estimated, or directly from satellite radar data (Esch et al., 2010). In this study, the buildings footprint information was available for the case study and building density was estimated in a grid of 30 m spatial resolution using GIS (Geographical Information Systems) analysis.

3.3 Impervious and Pervious Surface Fraction

Impervious and pervious surface fractions are the proportion of ground surface with impervious and pervious cover, respectively. Impervious and pervious surface fractions affect the albedo, the moisture availability and the heating/cooling rates. A large variety of remote sensing methods exist in literature to derive impervious and pervious surface fraction from EO data using different classification techniques (Weng, 2012). In this study, Landsat multispectral data was used to estimate the impervious and vegetation surface fraction (Mitraka et al., 2012). Four fundamental land cover components were assumed (i.e. vegetation, bright impervious, dark impervious and soil) and representative image collected spectra were used to invert the mixture problem using multiple endmembers. Impervious surface fraction was then estimated by combining the bright and dark impervious fractions at 30 m spatial resolution.

3.4 Mean Building/Tree Height

Mean building/tree height is the spatial average of building heights in an area of interest. It affects the surface albedo, flow regimes and heat dispersion above ground. The height of buildings and trees can be estimated from high spatial resolution DSM, given also information on the surface elevation. The finest and more accurate information on building/tree height can be derived using airborne LiDAR observations or high resolution stereoscopic imagery from airborne sensors (Stal et al., 2013). DSM can also be constructed from satellite radar data, with a few limitations over urban areas (Wegner et al., 2014). In this study, information on building/tree height was estimated using the high resolution DSM, produced by stereo-analysis of airborne imagery, removing the terrain using the DTM, to retrieve the objects' height. The geometric mean was estimated for each 30 m spatial resolution cell of a grid covering the study area.

3.5 Surface Albedo

Surface albedo represents the surface ability to reflect the incoming direct and diffused irradiance at all wavelengths and towards all possible angles. Albedo is calculated as the bi-hemispherical reflectance of a surface and varies between 0 and 1 (unitless). Albedo affects the surface radiational heating potential, varies with surface colour, wetness and roughness (Schaepman-Strub et al., 2006). Given the Bidirectional Reflectance Distribution Function (BRDF) of specific surface, its albedo can be estimated from EO data as the ratio of the total reflected energy of the surface to the total incident energy on the surface (Lucht et al., 2000). In this study, albedo was derived using the approach of (Liang, 2001) adjusted for Landsat-8 in 30 spatial resolution.

3.6 Identification of LCZ

The overall methodology for deriving delineating the LCZ is shown in Fig. 2a. The multiple sources of information used for estimating the different parameters resulted in products of different scales. Thus, there was a need to set a common scale of calculations to further proceed with the identification of possible LCZ. Moreover, there are restrictions in the definition of LCZ to ensure the homogeneity of the zone that was necessary to account for (Steward and Oke, 2012). A spatial resolution of 90 m was considered adequate for the purpose of this study, in accordance with the LCZ requirements and facilitating calculations with parameters derived from the Landsat-8 image (of 30 m spatial resolution).

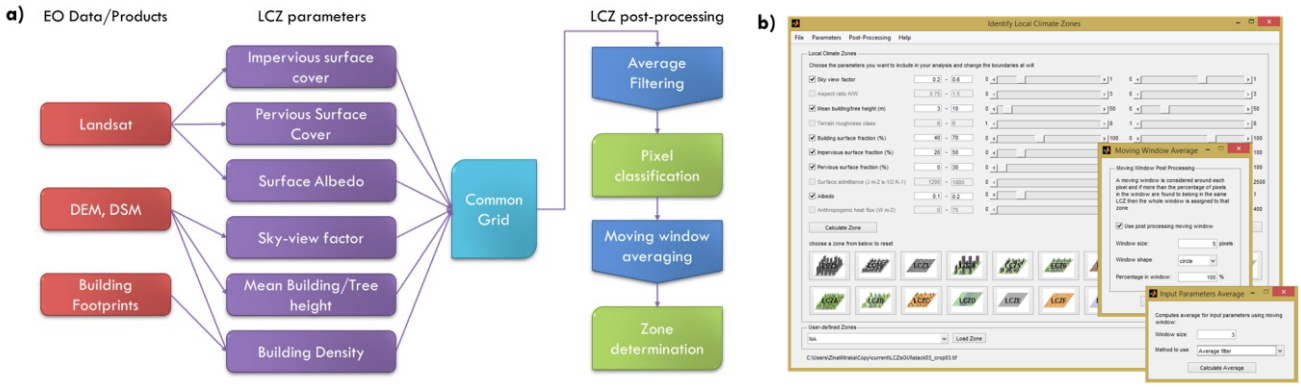

Fig. 2. (a) The LCZ identification scheme and (b) screenshots of the application developed to facilitate calculations.

Consequently, all derived parameters were averaged in a grid of 90 m × 90 m cell spatial resolution and each grid cell was classified, based on its sky-view factor, building density, impervious/pervious surface fraction, mean building/tree height, albedo, according to (Steward and Oke, 2012). For a geographic area to be identified as a LCZ it should have a minimum diameter of 400 – 1000 m. Thus, a 5 × 5 cells (450 m × 450 m) moving window was considered around each 90 m × 90 m grid cell and if more than 90% of the cells was found to belong in the same LCZ, the whole window was assigned to that zone. An application with a graphical user interface (Fig. 2b) was created to facilitate the identification of LCZ, provided the calculated parameters.

4. Results and discussion

The different parameters estimated from EO data are shown in Fig. 3. Those parameters were used as described above to identify possible LCZ in the study area. Two urban LCZ were identified for the case study of Heraklion presented in Fig. 4. Blue colour represents the LCZ3, while green the LCZ6. It is worth noticing here that just the urban zones of the LCZ classification were considered in this study. Moreover, the classification was based on the available parameters only, excluding for example the surface admittance or the anthropogenic heat flux, which are also crucial for the zones discrimination.

LCZ3 seems to describe quite well the reality in the respective part identified in the study area (blue in Fig. 4). This area is both commercial and residential and its buildings are in most cases attached or otherwise closely spaced. Although in the city centre there are some taller buildings (5-6 stories tall), the majority is 2-3 stories tall with an average building height found in the area around 5 m. The mean sky-view factor from the street level found around 0.55 which is considered reduced, but not significantly, since it is found close to the upper bound in the definition of LCZ3 (0.6). The main construction materials are concrete, brick and tile, but information of the surface admittance would further corroborate this claim. There is also lack of vegetated surfaces in this area, apart from some street trees and small parks (see Fig. 1). Although there is a normal demand for heating, there is a high demand for cooling in the city, during the summer season and moderate traffic flow. Both heating/cooling demand and traffic flow effects were not captured in this study, because no anthropogenic heat flux data were used.

LCZ6 matches the description of the respective area identified in Heraklion (green in Fig. 4). The area is the

periphery of the city of Heraklion and it is mainly a residential area. Buildings of maximum 3 stories tall are found here, with a mean sky-view factor of around 0.7. The construction materials used in this area are the same with the ones in the city core, but again the lack of surface admittance data prevented further discrimination. Much more vegetation cover is observed in this zone compared to LCZ3, both scattered trees and abundant plants. Heating demand is normal due to mild winters, cooling demand quite high during summer and traffic flow is generally low in this area. Again, to quantify these effects anthropogenic heat flux information is necessary.

The scope of this study is to outline a methodology for characterizing the LCZ by deriving each urban parameter using EO data and remote sensing science. More investigation is needed to come to conclusions about heat islands. Parameters like, the canyon aspect ratio, the terrain roughness, the surface admittance and the anthropogenic heat flux need to be considered in future studies.

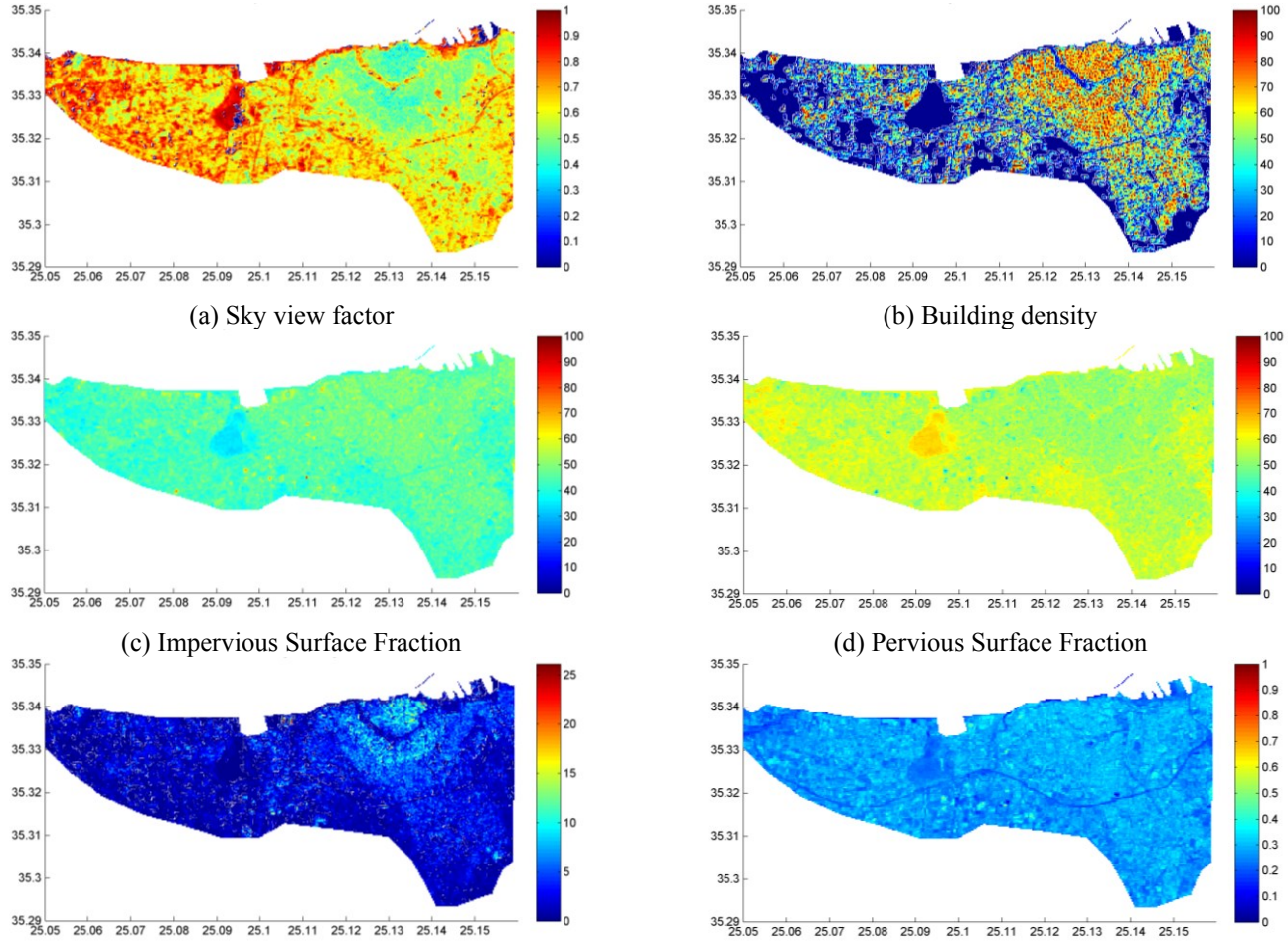

(a) Sky view factor (b) Building density

(c) Impervious Surface Fraction (d) Pervious Surface Fraction

(e) Mean Building/Tree Height (f) Surface Albedo

Fig. 3. Sky-view factor (a), building density (b), impervious (c) and pervious (d) surface fractions, mean building/tree height (e) and surface albedo (f), as estimated from the EO data.

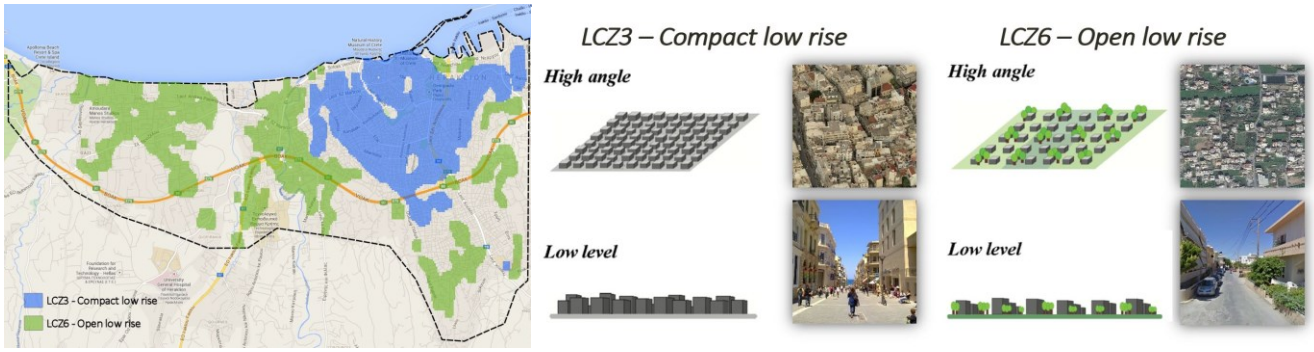

Fig. 4. The spatial extend of the two urban LCZ identified in the case study, overlayed to Google Maps (top). Blue corresponds to LCZ3, while green corresponds to LCZ6 and (bottom) their high angle and low level view (adapted by Steward and Oke (2012) and photos from Google Street-view and Bing Images).

5. Conclusions

This is considered as a first attempt to demonstrate how the exploitation of EO data can assist to quantify parameters related to the thermal behaviour of urban areas, with an ultimate goal to identify LCZ (Steward and Oke, 2012). Furthermore, the surface roughness class, the surface admittance and the anthropogenic heat flux can be derived using EO data and meteorological measurements. Future research includes advancing existing methods for parameters estimation and the exploitation of EO data for more LCZ parameters, like surface energy balance modelling for anthropogenic heat flux, with ultimate goal to develop a standard methodology for mapping LCZ.

Acknowledgment

The project leading to this application has received funding from the European Union's Horizon 2020 research and innovation programme under grant agreement No 637519.

References

Bechtel, B. et al., 2015. Mapping Local Climate Zones for a Worldwide Database of the Form and Function of Cities. *ISPRS International Journal of Geo-Information*, 4(1), pp.199–219.

Bechtel, B., Daneke, C., 2012. Classification of Local Climate Zones Based on Multiple Earth Observation Data. *IEEE Journal of Selected Topics in Applied Earth Observations and Remote Sensing*, 5(4), 1191–1202.

Chrysoulakis, N. et al., 2013. Sustainable urban metabolism as a link between bio-physical sciences and urban planning: The BRIDGE project. *Landscape and Urban Planning*, 112, 100–117.

Chrysoulakis, N., 2003. Estimation of the all-wave urban surface radiation balance by use of ASTER multispectral imagery and in situ spatial data. *Journal of Geophysical Research*, 108(D18), 4582.

Esch, T., Thiel, M., Schenk, A., 2010. Delineation of urban footprints from TerraSAR-X data by analyzing speckle characteristics and intensity information. *IEEE Transactions on Geoscience and Remote Sensing*, 48(2), 905–916.

Gamba, P., Lisini, G., Liu, P., 2012. Urban climate zone detection and discrimination using object-based analysis of VHR scenes. *Proceedings of the 4th GEOBIA, Rio de Janeiro - Brazil*, 70–74.

Grimmond, C.S.B. et al., 2010. Climate and More Sustainable Cities: Climate Information for Improved Planning and Management of Cities (Producers/Capabilities Perspective). *Procedia Environmental Sciences*, 1, 247–274.

Lelovics, E. et al., 2014. Design of an urban monitoring network based on Local Climate Zone mapping and temperature pattern modelling. Climate Research, 60, 51–62.

Liang, S., 2001. Narrowband to broadband conversions of land surface albedo I: Algorithms. *Remote Sensing of Environment*, 76, 213–238.

Lindberg, F., Grimmond, C., 2010. Continuous sky view factor maps from high resolution urban digital elevation models. *Climate Research*, 42(3), 177–183.

Lucht, W., Schaaf, C.B., Strahler, A.H., 2000. An algorithm for the retrieval of albedo from space using semiempirical BRDF models. IEEE Transactions on Geoscience and Remote Sensing, 38(2), 977–998.

Luyssaert, S. et al., 2014. Land management and land-cover change have impacts of similar magnitude on surface temperature. *Nature*, (April), 1–5.

Meirich, S., 2008. Mapping Guide for a European Urban Atlas. *GSE Land Information Services. GSE Land Consortium*. Available at: http://www.ftsnet.it/documenti/740/mapping guide for a european urban atlas_EEA.pdf

Mitraka, Z. et al., 2012. Improving the estimation of urban surface emissivity based on sub-pixel classification of high resolution satellite imagery. *Remote Sensing of Environment*, 117, 125–134.

Mitraka, Z. et al., 2015. Exploiting Earth Observation data products for mapping Local Climate Zones. In *Urban Remote Sensing Event (JURSE), 2015 Joint*. pp. 1–4.

Priestnall, G., Jaafar, J., Duncan, A., 2000. Extracting urban features from LiDAR digital surface models. *Computers, Environment and Urban Systems*, 24(2), 65–78.

Rigo, G., Parlow, E., 2007. Modelling the ground heat flux of an urban area using remote sensing data. Theoretical and Applied Climatology, 90(3-4), 185–199.

Schaepman-Strub, G. et al., 2006. Reflectance quantities in optical remote sensing—definitions and case studies. *Remote Sensing of Environment*, 103(1), 27–42.

See, L. et al., 2015. Developing a community-based worldwide urban morphology and materials database (WUDAPT) using remote sensing and crowdsourcing for improved urban climate modelling. In *Urban Remote Sensing Event (JURSE), 2015 Joint*. 1–4.

Skarbit, N., Gal, T., Unger, J., 2015. Airborne surface temperature differences of the different Local Climate Zones in the urban area of a medium sized city. In *Urban Remote Sensing Event (JURSE), 2015 Joint*. 1–4.

Stal, C. et al., 2013. Airborne photogrammetry and lidar for DSM extraction and 3D change detection over an urban area – a comparative study. International Journal of Remote Sensing, 34(4), 1087–1110.

Stewart, I.D., Oke, T.R., 2012. Local Climate Zones for Urban Temperature Studies. *Bulletin of the American Meteorological Society*, 93(12), 1879–1900.

Voogt, J., Oke, T.R., 2003. Thermal remote sensing of urban climates. *Remote Sensing of Environment*, 86(3), 370–384.

Wegner, J., Ziehn, J., Soergel, U., 2014. Combining High-Resolution Optical and InSAR Features for Height Estimation of Buildings with Flat Roofs. IEEE Transactions on Geoscience and Remote Sensing, 52(9), 5840–5854.

Weng, Q., 2012. Remote sensing of impervious surfaces in the urban areas: Requirements, methods, and trends. *Remote Sensing of Environment*, 117, 34–49.

Xu, W., Wooster, M.J., Grimmond, C.S.B., 2008. Modelling of urban sensible heat flux at multiple spatial scales: A demonstration using airborne hyperspectral imagery of Shanghai and a temperature–emissivity separation approach. *Remote Sensing of Environment*, 112(9), 3493–3510.